Origin and temperature dependence of the electric dipole moment in niobium clusters

Kristopher E. Andersen,[1] Vijay Kumar,[2,3,4] Yoshiyuki Kawazoe,[4] and Warren E. Pickett[1,*]

[1]*Department of Physics, University of California, Davis, California 95616-8677, USA*
[2]*Research Institute for Computational Sciences (RICS), National Institute of Advanced Industrial Science and Technology (AIST), AIST Tsukuba Central 2, Umezono 1-1-1, Tsukuba, 305-8568, Japan*
[3]*Dr. Vijay Kumar Foundation, 45 Bazaar Street, Chennai 600 078, India*
[4]*Institute for Materials Research, Tohoku University, 2-1-1 Katahira Aoba-ku, Sendai 980-8577, Japan*

The origin of spontaneous electric dipole moments and uncoupled magnetic moments, observed in niobium clusters below a size dependent critical temperature, are explained using first-principles electronic structure calculations. The calculated dipole moments for Nb_N ($N=2-15$) generally agree with the experiment, and support the interpretation that the electric dipole has a structural origin. A strong correlation is found between structural asymmetry, as quantified by the inertial moments and charge deformation density, and the electric dipole. For clusters with odd N, magnetocrystalline anisotropy is small in comparison to the rotational energy of the cluster, such that the spin magnetic moment ($1\mu_B$) is uncoupled to the cluster. Two potential mechanisms to explain the temperature dependence of the electric dipole are investigated. The excitation of harmonic vibrations is unable to explain the observed temperature dependence. However, classical simulations of the deflection of a cluster in a molecular beam show that thermal averaging reduces the asymmetry of the deflection profile at higher temperatures, which may affect the experimental observation of the electric dipole and polarizability. An experimental test is proposed to ascertain the importance of this effect.

I. INTRODUCTION

The recent observation of size dependent electric and magnetic moments in Nb_N clusters ($5 \leqslant N \leqslant 200$) and their temperature dependence has been discussed in the context of nascent superconductivity[1,2] and raises questions about the coupling between spontaneous electric dipoles and magnetism in nanoscale systems. One issue is the origin of the electric dipole in a homonuclear nanosystem, namely, what supports the charge separation at these length scales? Another issue is the change in the molecular beam deflection with temperature, which has been attributed to the change in the electric dipole in clusters formed at different temperatures. The inferred electric dipole moment is only seen in clusters formed below a size dependent critical temperature $T_c(N)$:[1] the nanoscale analogy of a ferroelectric transition. This temperature dependence could be of intrinsic origin, or it could be caused by external processes, such as the rotation of the cluster in the molecular beam. In this paper, first-principles electronic structure calculations are presented on niobium clusters that explain in a simple way the origin of the electric dipole in nanosystems. The calculated electric dipoles are in good agreement with experiments for the small cluster sizes ($2 \leqslant N \leqslant 15$) studied. Classical simulations of the rotational dynamics also reveal that thermal averaging may affect the experimental analysis, and an experimental test is proposed to determine the importance of this effect.

Permanent electric dipole moments have been observed in molecular beam experiments by Moro *et al.* for Nb clusters, as well as clusters of Ta, V, and Al.[1] Modeling the distribution of Nb clusters with a permanent electric dipole moment using Boltzmann statistics they obtained size dependent critical temperatures $T_c(100)=10$ K and $T_c(11)=110$ K,[1] which

reveal that it is easier to observe electric dipole moments in small clusters at low temperatures. Subsequent molecular beam experiments with a Stern-Gerlach magnet have shown that the paramagnetic response is also unusual, in which the spin moment ($1\mu_B$ in odd N clusters due to an odd number of electrons) is uncoupled to the cluster.[2] Furthermore, the dielectric and paramagnetic response appear to have a correlated temperature dependence,[1,2] in which both the uncoupled spin moment and electric dipole moment are only observed below $T_c(N)$.

The correspondence of $T_c(N)$, approximately 10 K for large N, and the 9.2 K superconducting critical temperature of bulk Nb prompted speculation that the electric dipole moment in niobium clusters was associated with nascent superconductivity.[1,2] Although superconductivity in metallic nanoparticles has been formally defined by Andreev,[3] it has yet to be observed in tunneling experiments on (much larger) Al nanoparticles.[4] (See also the review of Ref. 5.) Furthermore, the similar temperature dependence of the spin and electric dipole moments may be related to the rotational dynamics of the clusters in a molecular beam.

Permanent electric dipole moments are commonly found in heteronuclear molecular systems. However, disproportion into charged ions is energetically disfavored in a homonuclear cluster, though small charge transfers could be possible due to the presence of inequivalent sites. Therefore, it is challenging to envision what chemical forces support the underlying charge separation in clusters of metal atoms that are going to become metallic—and hence support no charge separation—as their size increases. The Falicov-Kimball model predicts a ferroelectric state in metals of purely electronic origin[6] due to a coupling between electrons with s and p angular character. However, the applicability of this model

is uncertain in niobium clusters since states near the Fermi energy are of primarily *d* character (see Sec. V). Interestingly, quantum effects can produce an electric dipole in symmetric clusters where it is classically forbidden.[7,8] Although quantum effects may explain the electric dipole in small clusters (e.g., Nb_3) they should diminish with the mass of the cluster, whereas in experiment electric dipoles are still observed in clusters with hundreds of atoms.

We have shown from first-principles calculations on Nb_N for $N=2-15$ that the electric dipole moments can be explained by structural asymmetry,[9] and recently, this conclusion has also been reached by Fa *et al.* who performed calculations on $N=2-52$.[10] Also, classical simulations, based on the calculated dipole moment and structure, support the conclusion that the electric dipole may persist at higher temperatures, but is more difficult to detect experimentally due to additional thermal averaging caused by rotational dynamics.[9]

In this paper, we discuss the calculations of Ref. 9 in more detail and elaborate on the relationship between the spin and electric moments and the coupling between the spin moment and the cluster. We believe the following analysis offers a reasonable description of the experimental trends and is appealing in its simplicity. Although our calculations are on small Nb clusters ($N \leq 15$) of a certain geometry, we believe that many aspects of our interpretation extend to larger clusters which are computationally more demanding and to clusters of other elements.

Computational methods are discussed in Sec. II. In Sec. III, the calculated electric dipole moment is compared to experiment and previous calculations, and in Sec. IV it is interpreted in terms of the asymmetry of the cluster, where asymmetry is quantified using the principal moments of inertia and charge deformation density. The relationship between the electric dipole moment and spin moment is presented in Sec. V. In Sec. VI, the coupling of the spin moment to the cluster is discussed, which is mediated by spin-orbit coupling, and in Sec. VII the temperature dependence of the electric dipole moment is investigated by analyzing the vibrational and rotational dynamics of the cluster.

II. METHODS

First-principles electronic structure calculations were done using the planewave, norm-conserving pseudopotential method as implemented in ABINIT 4.2.4,[11,40] which relies on efficient fast Fourier transform[12] and conjugate-gradient minimization[13,14] algorithms. The Perdew-Burke-Ernzerhof generalized gradient approximation (GGA) functional[15] was used to approximate the exchange and correlation potential, and a spin polarized functional was used for clusters with odd *N* and the dimer.

The niobium pseudopotential was generated with FHI98PP (Ref. 16) using the Troullier-Martins method[17] and the same GGA functional. 4*s* and 4*p* semicore states were included in the pseudopotential, and were necessary to reproduce the band structure of bulk Nb obtained from the all-electron, linearized augmented plane wave method. A 45 H cutoff energy $\mathcal{E}_{cut}$ was used to converge the plane wave basis set, and a convergence of the electronic density was based on

the relative error of the input and output potentials using a tolerance of 10^{-9}.

The cluster was placed in a simple cubic supercell of 15 Å, and only the Γ point was used for Brillouin zone integrations. Because the clusters are mutually isolated, this is equivalent to doing a full potential cluster calculation.

The lowest energy structures obtained by Kumar and Kawazoe[18] in the size range of $2 \leq N \leq 15$ as well as known isomers with binding energies within 25 meV/atom were studied. Isomers were found for $N=6$, 9, 11, and 12. Throughout this work letters are used to label isomers in alphabetical order. For example, Nb_{6a} is the lowest energy structure and Nb_{6b} is higher in energy. The isomers Nb_{6b}, Nb_{9b}, Nb_{11b}, and Nb_{12b} have binding energies 18, 3, 12, and 20 meV/atom lower than the corresponding *a* structures, respectively. Although isomers have been observed experimentally for $N=9$, 11, and 12 (Refs. 19–23) and cluster ions of $N=11$ and 12,[24,25] we are not aware of any experimental report for $N=6$. In addition, no energetically competitive structure was found for Nb_{10} (nor in other theoretical studies[26,27]), although an isomer of Nb_{10} has been reported.[22,23]

Structural optimization was performed to minimize the maximum component of force on each atom to less than 10 meV/Å. Furthermore, additional geometries were investigated to search for new, energetically favorable structures. This search yielded lower energy structures for $N=12$ and 13, which are referred to as Nb_{12a} and Nb_{13}.[41] (The Nb_{13} structure is the same as in Refs. 9 and 28.) Except for these two exceptions, the structures used here are the same as those reported by Kumar and Kawazoe[18] with only minor changes in bond lengths.

A. Electric dipole moment

The electric dipole moment $\boldsymbol{\mu}$ is calculated using the total charge density $\rho(\boldsymbol{r})$

$$\boldsymbol{\mu} = \int_{\Omega} \boldsymbol{r}\rho(\boldsymbol{r})d^3r = \sum_{i\sigma} \boldsymbol{\mu}^e_{i\sigma} + \boldsymbol{\mu}^{\text{ion}}, \qquad (1)$$

where the integration is over the supercell volume Ω.

$$\boldsymbol{\mu}^e_{i\sigma} = -ef_{i\sigma} \int_{\Omega} \boldsymbol{r}n_{i\sigma}(\boldsymbol{r})d^3r \qquad (2)$$

is the contribution to the total dipole moment from the electron density $n_{i\sigma}(\boldsymbol{r})$ of the *i*th electronic state with spin σ and occupation $f_{i\sigma}$, and

$$\boldsymbol{\mu}^{\text{ion}} = \sum_{n} Z_n \boldsymbol{r}_n \qquad (3)$$

is the contribution from the ions (i.e., the nuclear plus the core electron charge) with the pseudocharge Z_n located at the position $\boldsymbol{r}_n$.

Since the electron density $n_{i\sigma}(\boldsymbol{r}) = \Sigma_{\boldsymbol{G}} n_{i\sigma\boldsymbol{G}} e^{i\boldsymbol{G}\cdot\boldsymbol{r}}$ can be obtained as a Fourier series over reciprocal lattice vectors $\boldsymbol{G}$, the integral in (2) can be done analytically. The general form of the solution is

$$\boldsymbol{\mu}_{i\sigma}^{e}(\boldsymbol{r}) = -ef_{i\sigma}\Omega\sum_{\boldsymbol{G}} n_{i\sigma\boldsymbol{G}}(c_1\boldsymbol{R}_1 + c_2\boldsymbol{R}_2 + c_3\boldsymbol{R}_3), \qquad (4)$$

where $\boldsymbol{R}_j$ ($j=1-3$) are the direct lattice vectors and c_j are complex constants arising from the integration.

The expressions for c_j depend on where the cluster is within the supercell since the integration domain Ω must properly enclose the charge density. In practice, only two cases need to be considered. First is when the cluster is near the center of the supercell (odd symmetry) such that $\int_\Omega d^3 r \rightarrow \Omega \int_0^1 \int_0^1 \int_0^1 du\, dv\, dw$. Then

$$c_1^{\text{odd}} = \begin{cases} \dfrac{1}{2}\delta_{n_2,0}\delta_{n_3,0} & \text{if } n_1 = 1, \\[2mm] \dfrac{1}{i2\pi n_1}\delta_{n_2,0}\delta_{n_3,0} & \text{otherwise,} \end{cases} \qquad (5)$$

$$c_2^{\text{odd}} = \begin{cases} \dfrac{1}{2}\delta_{n_3,0}\delta_{n_1,0} & \text{if } n_2 = 0 \\[2mm] \dfrac{1}{i2\pi n_2}\delta_{n_3,0}\delta_{n_1,0} & \text{otherwise} \end{cases} \qquad (6)$$

$$c_3^{\text{odd}} = \begin{cases} \dfrac{1}{2}\delta_{n_1,0}\delta_{n_2,0} & \text{if } n_3 = 0 \\[2mm] \dfrac{1}{i2\pi n_3}\delta_{n_1,0}\delta_{n_2,0} & \text{otherwise.} \end{cases} \qquad (7)$$

Second is when the cluster is near the corner of the supercell (even symmetry) such that

$$\int_\Omega d^3 r \rightarrow \Omega \int_{-1/2}^{1/2} \int_{-1/2}^{1/2} \int_{-1/2}^{1/2} du\, dv\, dw.$$

Then

$$c_1^{\text{even}} = \begin{cases} 0 & \text{if } n_1 = 0 \\[2mm] \dfrac{\cos(\pi n_1)}{i2\pi n_1}\delta_{n_2,0}\delta_{n_3,0} & \text{otherwise} \end{cases}, \qquad (8)$$

$$c_2^{\text{even}} = \begin{cases} 0 & \text{if } n_2 = 0, \\[2mm] \dfrac{\cos(\pi n_2)}{i2\pi n_2}\delta_{n_3,0}\delta_{n_1,0} & \text{otherwise} \end{cases} \qquad (9)$$

$$c_3^{\text{even}} = \begin{cases} 0 & \text{if } n_3 = 0 \\[2mm] \dfrac{\cos(\pi n_3)}{i2\pi n_3}\delta_{n_1,0}\delta_{n_2,0} & \text{otherwise} \end{cases}. \qquad (10)$$

In Eqs. (5)–(10), the integers n_j specify the reciprocal lattice vector $\boldsymbol{G}=n_1\boldsymbol{G}_1+n_2\boldsymbol{G}_2+n_3\boldsymbol{G}_3$.

Two key parameters governing the quality of the calculations are the plane wave cutoff energy $\mathcal{E}_{\text{cut}}$ and the supercell size. In Table I, the total energy and dipole moment for Nb_{12b} are given for larger values of $\mathcal{E}_{\text{cut}}$, and show negligible change in the electric dipole.

TABLE I. Convergence of the total energy (H) and magnitude of the dipole moment (D) with respect to the plane wave cutoff energy $\mathcal{E}_{\text{cut}}$ (H) for Nb_{12b}.

$\mathcal{E}_{\text{cut}}$	Total energy	Dipole moment
45	−683.5452	2.6764
55	−683.5472	2.6764
65	−683.5540	2.6761

One test of the convergence of the calculation with respect to the supercell size is to displace the cluster's center of mass a small distance. For a perfectly converged calculation (large enough $\mathcal{E}_{\text{cut}}$ and supercell), such a displacement should not change the dipole moment. Displacing the center of mass of Nb_{12b} 0.2 Å changed the calculated dipole moment less than 0.1%, which indicates that the charge density is accurately represented.

B. Linear response

The linear response of the electronic charge density to infinitesimal atomic displacements and homogeneous electric fields was calculated using the methods described by Gonze and Lee.[29,30] The principal quantities obtained are the normal mode vibrational frequencies and dynamical (or Born effective) charge tensors.

The dynamical charge tensor $Z_{\alpha\beta}^{n}$ (with units of charge) is the second-order derivative of the total energy $\mathcal{E}$

$$Z_{\alpha\beta}^{n} = \frac{\partial^2 \mathcal{E}}{\partial E_\alpha \partial \tau_{n\beta}} \qquad (11)$$

with respect to the applied electric field $\boldsymbol{E}$ and the displacement $\boldsymbol{\tau}_n$ of the nth atom. (α and β are the Cartesian indices x, y, and z.) For clusters, $Z_{\alpha\beta}^{n}$ is also related to the change in the electric dipole moment

$$Z_{\alpha\beta}^{n} = \frac{\partial \mu_\alpha}{\partial \tau_{n\beta}}, \qquad (12)$$

and physically describes the induced dipole moment caused by the response of the atoms to an applied electric field.

C. Spin-orbit interaction

The spin-orbit coupling interaction strength was calculated using the projector augmented-wave method[31,32] as implemented in the VASP version 4.6.26,[33,34] with "high precision" and a wave function expansion cutoff energy $\mathcal{E}_{\text{cut}} = 13$ H.

The strength of the spin-orbit interaction V_{SO} is proportional to $\boldsymbol{L}\cdot\boldsymbol{\sigma}$, where $\boldsymbol{L}$ and $\boldsymbol{\sigma}$ are the angular and spin moments, respectively. For clusters with odd N a nonzero spin moment is expected due to the odd number of electrons, and ground state spin polarized calculations (without spin-orbit coupling) found the magnitude of the spin moment to be $\sigma = 1\mu_B$ for all odd clusters studied (see Table II).

To determine V_{SO}, the quantization axis of the spin moment $\hat{\boldsymbol{\sigma}}$ on each atom (with *collinear* moments) was then

TABLE II. Point group symmetry, principal moments of inertia $I_1 - I_3$ (M_{Nb} Å^2), electric dipole moment μ (D), and spin moment σ (μ_B) for Nb$_N$. For clusters with an electric dipole moment, the projection of the moment along the direction of each principle axis is given by the angles $\theta_1 - \theta_3$ (degrees). Letters denote higher energy isomers in alphabetical order. (1 $M_{Nb} = 1.5427 \times 10^{-25}$ kg).

N	Symmetry	I_1 (θ_1)	I_2 (θ_2)	I_3 (θ_3)	μ	σ
2	C_∞	0.00	2.21	2.21	0.0	2
3	C_{2v}	2.57 (0.0)	3.00 (90.0)	5.56 (90.0)	0.4	1
4	T_d	6.33	6.33	6.33	0.0	0
5	$\approx C_{2v}$	7.42 (89.7)	11.05 (87.1)	11.66 (3.0)	0.6	1
6a	$\approx C_{2v}$	10.37 (87.3)	15.92 (4.2)	17.65 (86.8)	0.3	0
6b	$\approx C_{2v}$	11.39 (90.7)	14.36 (0.7)	18.44 (90.0)	1.2	0
7	C_1	16.62 (33.0)	17.16 (103.2)	22.85 (60.4)	0.8	1
8	$\approx C_{2v}$	21.13 (180.0)	23.42 (90.0)	27.46 (90.0)	0.2	0
9a	$\approx$ mirror plane	28.76 (176.9)	29.09 (92.4)	32.06 (88.0)	0.3	1
9b	$\approx C_2$	24.97 (89.3)	30.23 (88.9)	36.79 (178.7)	1.0	1
10	$\approx D_{4d}$	32.54	38.03	38.03	0.0	0
11a	$\approx C_2$	34.32 (91.9)	48.33 (89.4)	57.75 (178.0)	2.8	1
11b	C_1	38.02 (83.5)	43.72 (96.8)	59.10 (9.4)	2.5	1
12a	$\approx C_{2v}$	46.61 (91.0)	53.27 (1.0)	57.02 (89.8)	1.7	0
12b	C_1	42.85 (78.6)	54.96 (67.4)	63.90 (25.6)	2.7	0
13	C_1	50.89 (81.6)	61.51 (124.1)	75.15 (35.4)	1.7	1
14	$\approx C_6$	61.06 (90.5)	66.62 (89.9)	81.27 (0.5)	1.6	0
15	$\approx O_h$	73.30	76.19	76.20	0.0	1

varied, and the difference in total energy was obtained relative to a reference state with the spin moment aligned with the electric dipole moment axis $\hat{\boldsymbol{\mu}}$.

III. ELECTRIC DIPOLE MOMENT

The calculated permanent electric dipole moments are compared in Fig. 1 with the experimental data[1] and calculations by Fa *et al.*[10] In the experiment, the measured dipole
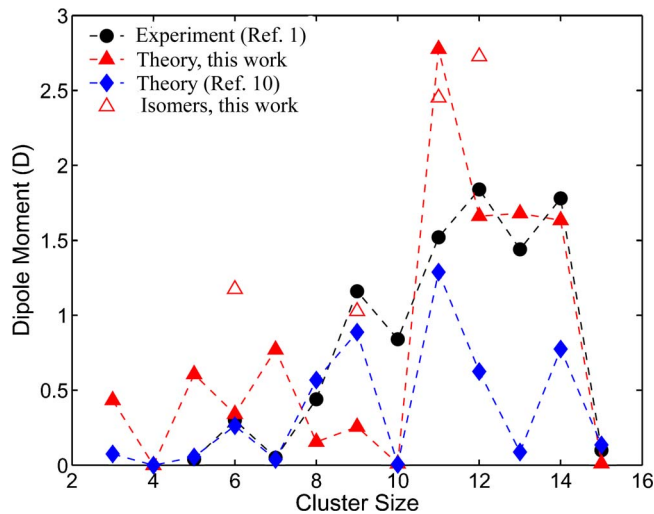

FIG. 1. (Color online) Comparison of the calculated electric dipole moment and the "low-temperature" (50 K) experimental data. (1 D = 0.2082 eÅ).

moment increases as the temperature at which the clusters are formed is lowered;[1] the data in Fig. 1 correspond to Nb clusters emitted after reaching the thermal equilibrium with He gas at 50 K. Considering the many uncertainties in presenting such a comparison (to be discussed), the level of agreement is satisfying. Despite some exceptions, moderate moments are generally found for $N = 3-9$, large moments for $N = 11-14$, and essentially zero moments for $N = 4, 10$, and 15.

One notable disagreement between theory and experiment is seen for Nb$_{10}$. However, analysis of the experimental data taking into account the fraction of clusters with a permanent moment at different temperatures suggests the "ferroelectric component is essentially absent for $N = 2, 4, 10, 15$,"[1] which is in excellent agreement with both theoretical calculations.

The comparison in Fig. 1 also reveals a disagreement between the two theoretical calculations, the source of which could extend from either the use of different atomic structures or different theoretical approximations. To estimate the level of agreement that might be expected between different calculations within the framework of the density functional theory, but using different basis sets, pseudopotentials, and/or exchange-correlation functionals, we compare in Fig. 2 the calculated dipole moments in this work with those of Ref. 9, which uses the same structures. Overall, the level of agreement is found to be within approximately 20% or a few tenths of a debye.

In Fig. 1 the differences between the theoretical calculations are often greater than 20%, and indeed, are as large as a factor of 20 for Nb$_7$ and Nb$_{13}$. However, excellent agreement is found for the symmetric clusters Nb$_4$, Nb$_{10}$, and
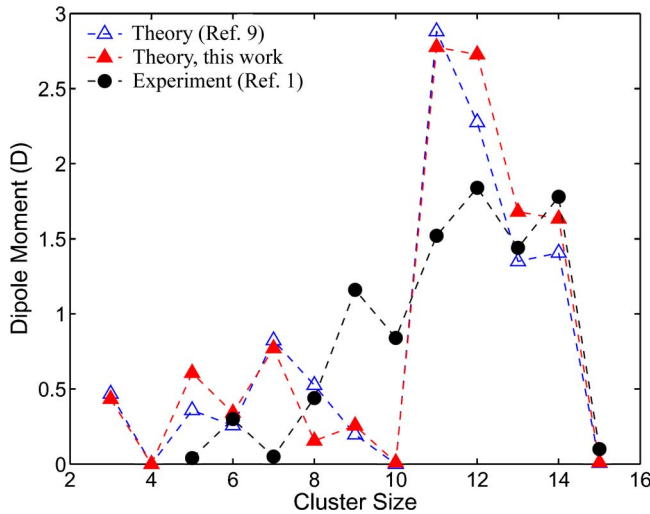
FIG. 2. (Color online) Comparing the numerical calculation of the electric dipole moment using different codes but the same atomic structures. The experimental data are shown as a reference.

FIG. 3. (Color online) Two clusters with approximate symmetry $Nb_{10}(\approx D_{4d})$ and $Nb_{15}(\approx O_h)$ and no electric dipole moment. The "bonds" only illustrate the symmetry of the cluster.

Nb_{15}, and good agreement is seen for Nb_6 (with the *a* isomer) and Nb_9 (*b* isomer). For $N=2-12$ Fa *et al.* found structures similar to those used in this work, except for Nb_8.[10] We therefore presume that the disagreement seen for Nb_5, Nb_7, and Nb_{11} is related in part to differences in the numerical calculations and in part to subtle structural differences. In some cases we find that modest changes in the atomic structure produce relatively large changes in the calculated electric dipole. For Nb_8, the structural relaxation performed in this work led to a change in the electric dipole moment from 0.5 to 0.2 D, as shown in Fig. 2, even though the atomic structure changed only slightly. For instance, the principal moments of inertia changed from (21.24, 23.63, 27.67) to (21.13, 23.42, 27.46) M_{Nb} Å^2. This strong structural dependence for the electric dipole moment of Nb_8 is caused by an approximate symmetry axis. A similar situation occurs for Nb_5.

For $N=13-15$, Fa *et al.* found icosahedral growth,[10] whereas Kumar and Kawazoe report layered hexagonal growth.[18] Although several calculations exist for clusters with $N=3-10$,[10,18,26,27,35] only these two studies extend beyond $N=10$. The experimental comparison in Fig. 1 supports layered hexagonal growth in this size range, but further independent comparisons between experiment and theory would help to establish the atomic structures.

IV. STRUCTURAL ASYMMETRY

The (lack of) symmetry of a cluster is strongly correlated with its electric dipole moment. In general, inversion symmetry is sufficient to prohibit the formation of an electric dipole, but in clusters and molecules, the lower D point group symmetry is sufficient when quantum effects are negligible.[8] Of the clusters studied, only Nb_2 and Nb_4 (a regular tetrahedron, T_d) are forbidden to have an electric dipole by symmetry.

However, two of the clusters studied Nb_{10} and Nb_{15}, shown in Fig. 3, are nearly symmetric and have negligible
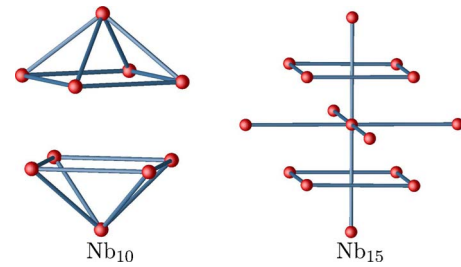
moments. In the case of Nb_{10}, the structure resembles two oppositely oriented square pyramids with a relative rotation of 37°. If the relative rotation was instead 45°, the structure would have D_{4d} symmetry and the electric dipole would be forbidden. For Nb_{15}, the structure is a distorted fragment of bcc Nb, an octahedron with two distorted squares along one axis. The distortion of each "square" is out of the plane, so the object is more precisely described as two edge-sharing isosceles triangles. Without the out of plane distortion, Nb_{15} would have O_h symmetry, which includes inversion.

The structures of the clusters are shown in Fig. 4 with the dipole moments and principal axes of inertia, and their approximate symmetries are given in Table II. Nb_5 and Nb_7 are distorted trigonal and pentagonal bipyramids, respectively. In symmetric structures the dipole moment would be zero in both these cases, but the distortions lead to relatively small dipole moments. Both these structures are relevant for the growth of larger clusters. The two isomers of Nb_6 can be described in terms of tetrahedral packing while Nb_8, Nb_{9a}, and Nb_{10} arise from bi-, tri-, and tetra-capped prism structures, respectively. Nb_{9b} can be considered a pentagonal bipyramid capped with a dimer; accordingly there is mirror symmetry in a plane bisecting this dimer, which contains the dipole moment. In Nb_{11a} there are two pentagonal bipyramids fused at a face. The dipole moment passes through this face and reflects the symmetry of this cluster. Nb_{11b} can be described as a capped hexagon connected to a rhombus. We optimized a capped hexagon for Nb_7 but it distorts significantly and lies higher in energy. Capped pentagonal pyramids can be seen in Nb_{12a}, while Nb_{12b} can be considered to have two pentagonal bipyramids fused at an edge and capped by an atom. Therefore, there is an approximate mirror plane in this structure. Structures of $N=13-15$ are best described in terms of hexagons, as seen in Fig. 4. Overall, these results show that pentagon based structures are energetically favored for $N=7-12$ (one can see pentagons in Nb_{9a} and Nb_{10} also), while hexagon based structures become lower in energy for $N>12$.

One measure of the asymmetry of the cluster can be obtained from the principal moments of inertia $I_1 \leq I_2 \leq I_3$ (Table II). The spread of the inertial moments $\Delta I = I_3 - I_1$ is strongly correlated with the magnitude of the electric dipole.[9] In addition, the *direction* of the electric dipole moment tends to align with one of the principal axes of inertia as shown in Fig. 4. The angles θ_1, θ_2, and θ_3 corresponding to the projection of the electric dipole onto each principal axis, respec-
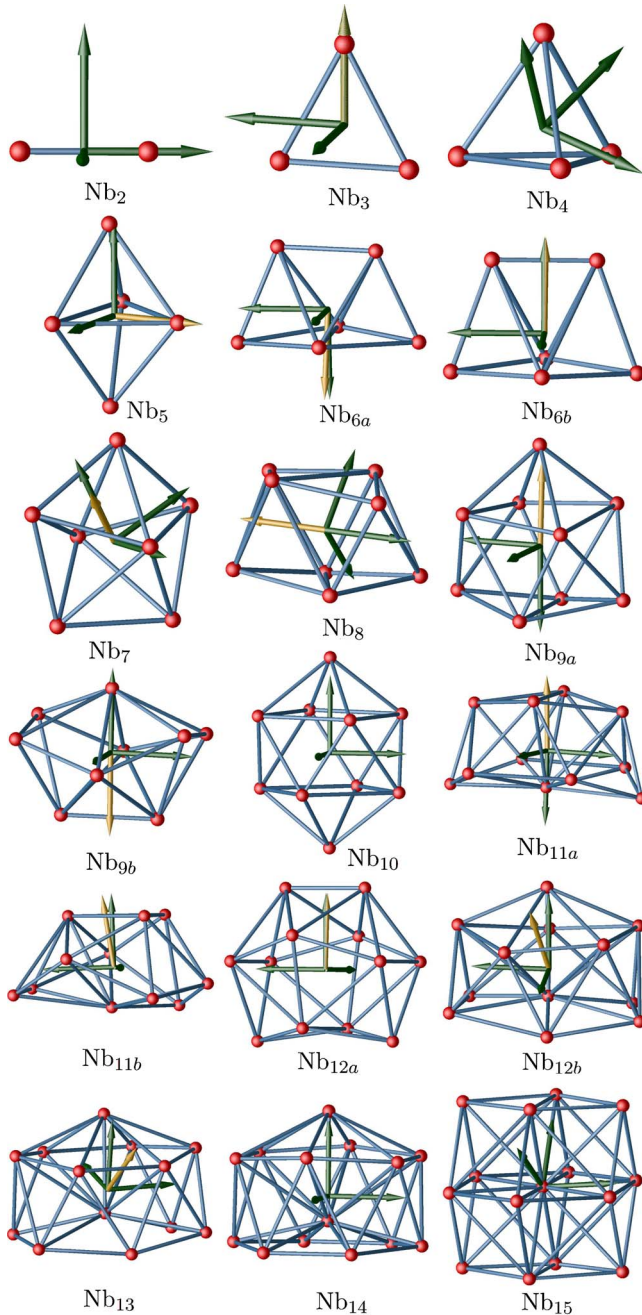
FIG. 4. (Color online) Principal axes of inertia (in green) and electric dipole moments (gold). The direction of the electric dipole tends to align with a principal axis of inertia (see Table II). Bonds are drawn if two atoms are within 10% of the nearest neighbor atomic separation in bulk Nb, 2.86 Å.

tively, are given in Table II. For many of the clusters with a large electric dipole (i.e., $N=11-14$) the moment tends to align with the axis corresponding to the largest principal moment of inertia I_3, although Nb_{12a} is an exception. (In this latter case, the electric dipole is nearly aligned with the axis corresponding to I_2.) The alignment of the electric dipole and a principal axis signifies there is a preferred axis in many of these clusters. This is caused by the predominance of approximate C_2 symmetry, and supports the conclusion that the growth of Nb_N clusters is layered.
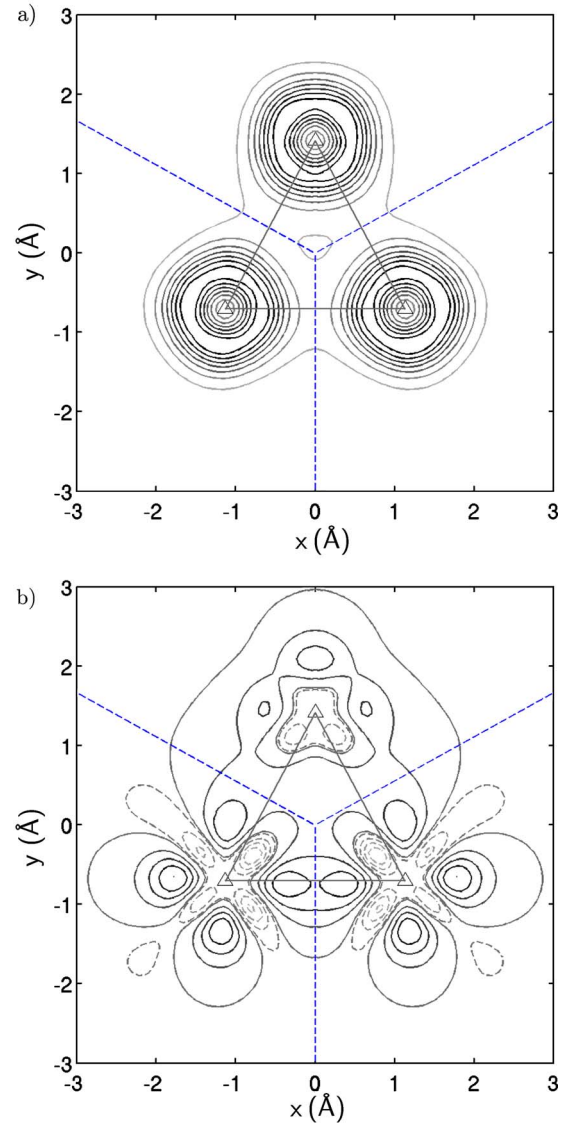

FIG. 5. (Color online) Nb_3 (a) total charge density and (b) charge deformation density. The Voronoi cell around each atom ($\triangle$) is outlined by dashed lines. In (b), the solid (dashed) contour lines indicate where charge accumulates (is depleted) during the formation of bonds. Symmetry restricts the electric dipole moment to lie along the y axis.

A. Illustrative case: Nb₃

In order to understand the origin of the electric dipole, it is advantageous to begin with Nb_3, which has many qualitative similarities to the larger clusters with higher symmetry. The structure of Nb_3 is an acute isosceles triangle with bond lengths of 2.27 and 2.40 Å and bond angles of 61.9° and 56.2°. Two mirror planes restrict the electric dipole to an axis. In Fig. 5, the dipole moment points in the $+y$ direction from the origin.

The existence of an electric dipole (0.4 D) implies that each Nb atom has some ionic character. In general, determining the effective charge of each atom is ill-defined because there is no unique way to define the volume of an atom and the charge integral is sensitive to this partitioning. However,

for Nb_3 symmetry implies an effective charge of $-q/2$ for each atom along the short bond and $+q$ for the remaining atom, where $q > 0$ is anticipated because an excess of negative charge accumulates along the short bond.

A Voronoi cell decomposition of the charge density finds $q = 0.04e$, and is consistent (within 10%) with the magnitude of the calculated electric dipole. The total charge density and the boundaries of the Voronoi cells are shown in Fig. 5(a). A fine, cubic mesh with 1024 grid points along each axis was needed to resolve the boundary between cells.

In a homonuclear cluster, no charge transfer might be expected, especially for Nb where directional, covalent bonding between d electrons characterizes the bulk. Is this small $\sim 10me$ amount of charge transfer unusual? Another homonuclear molecule ozone, O_3, has a comparable dipole moment of 0.6 D and an effective charge on each O atom of $0.08e$ is estimated using the geometry of the molecule. This magnitude of charge transfer is comparable to Nb_3. In ozone, however, the asymmetry of the structure, an obtuse isosceles triangle, arises from the directional bonding between p electrons. In contrast, the d electron bonding in Nb_3 favors a compact, acute isosceles structure.

B. Charge deformation

The relationship between the electric dipole and the directional bonding between Nb atoms is seen in the charge deformation density, which is the total charge density of the cluster minus the charge density of isostructural (spherically symmetric) neutral atoms. Since subtracting any neutral, spherically symmetric charge density at each atomic site does not change the net electric dipole, the dipole moment of the charge deformation density is equal to the dipole moment of the cluster. The deformation density conveys how charge redistributes when bonds are formed. The sign of the charge deformation density can be positive or negative, where negative (positive) values correspond to regions where charge is accumulated (depleted) during bonding.

The charge deformation density is shown in Fig. 6 for Nb_2-Nb_{15} at isosurfaces of ± 0.24 $e/\text{Å}^3$. A 2D projection of the deformation density for Nb_3 is shown in Fig. 5(b). Two qualitative features can be discerned. First is the formation of covalent bonds and the associated lobes of charge from the occupied $4d$ orbitals. Second, some charge is pushed outward at each surface site due to Coulomb repulsion. Clusters with a negligible electric dipole Nb_4, Nb_{10}, and Nb_{15} have a deformation density that is primarily intra-atomic, whereas other clusters have an asymmetric charge distribution and more covalent character.

V. STATE AND SPIN DECOMPOSITION

In order to understand which electronic states contribute to the electric dipole moment $\boldsymbol{\mu}$, we calculated contributions $\boldsymbol{\mu}_{i\sigma}^e$ from each electronic state i with spin σ and $\boldsymbol{\mu}^{\text{ion}}$ from the nuclei following from (1). Although the total electric dipole moment $\boldsymbol{\mu}$ is independent of the chosen origin, the contributions $\boldsymbol{\mu}_{i\sigma}^e$ and $\boldsymbol{\mu}^{\text{ion}}$ are not: only their vector sum is invariant. For simplicity, we choose the origin to be the center of mass
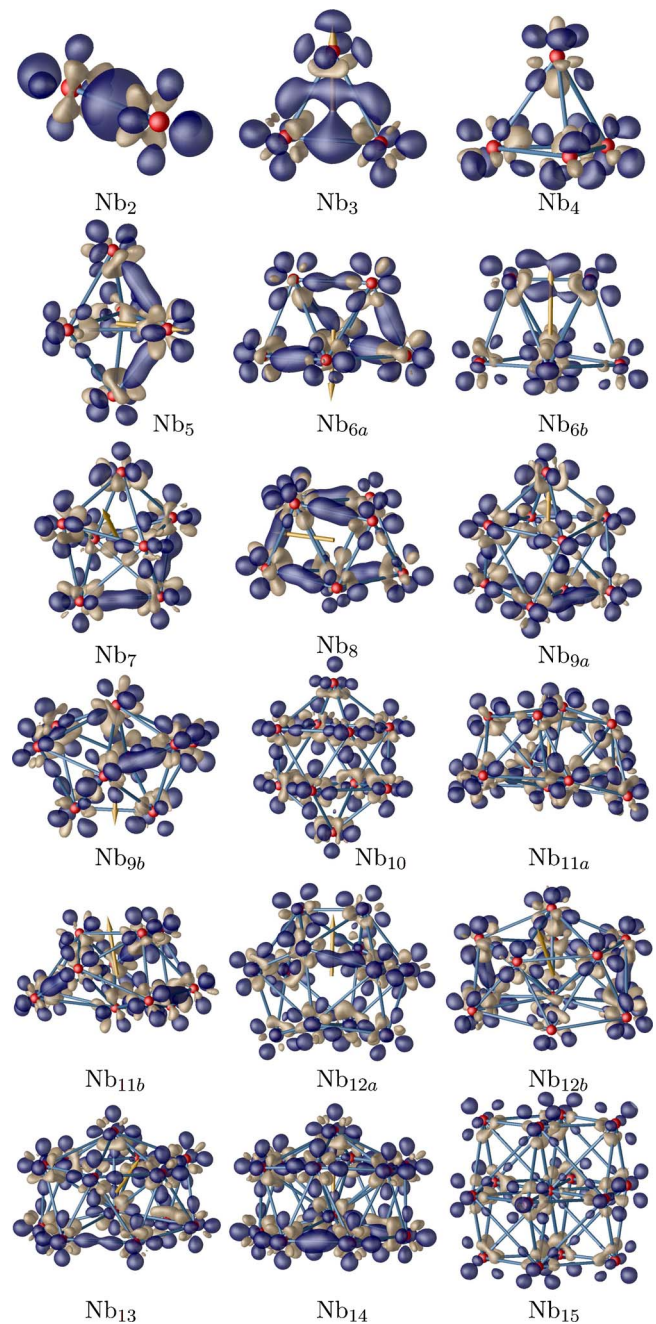

FIG. 6. (Color online) The charge deformation density. The negative isosurface (in blue) shows where charge accumulates during the formation of bonds. Likewise, the positive (gray) isosurface shows where the charge is depleted. More asymmetry is observed in clusters with a large electric dipole (e.g., Nb_{11}-Nb_{14}).

of the cluster such that $\boldsymbol{\mu}^{\text{ion}} = 0$; this choice does not affect the following discussion.

The state decomposed moments are shown pictorially in Fig. 7, where each state dipole $\boldsymbol{\mu}_{i\sigma}$ is represented as a vector originating from the center of mass of the cluster. The symmetry of the cluster is reflected in the state decomposition. In general, many states contribute in a nontrivial way (e.g., Nb_{13}), but in some cases an approximate symmetry plane (Nb_5, Nb_{6a}, Nb_{9a}, Nb_{9b}, Nb_{11a}, Nb_{12a}, and Nb_{14}) or axis (Nb_3, Nb_{6b}, and Nb_8) exists.
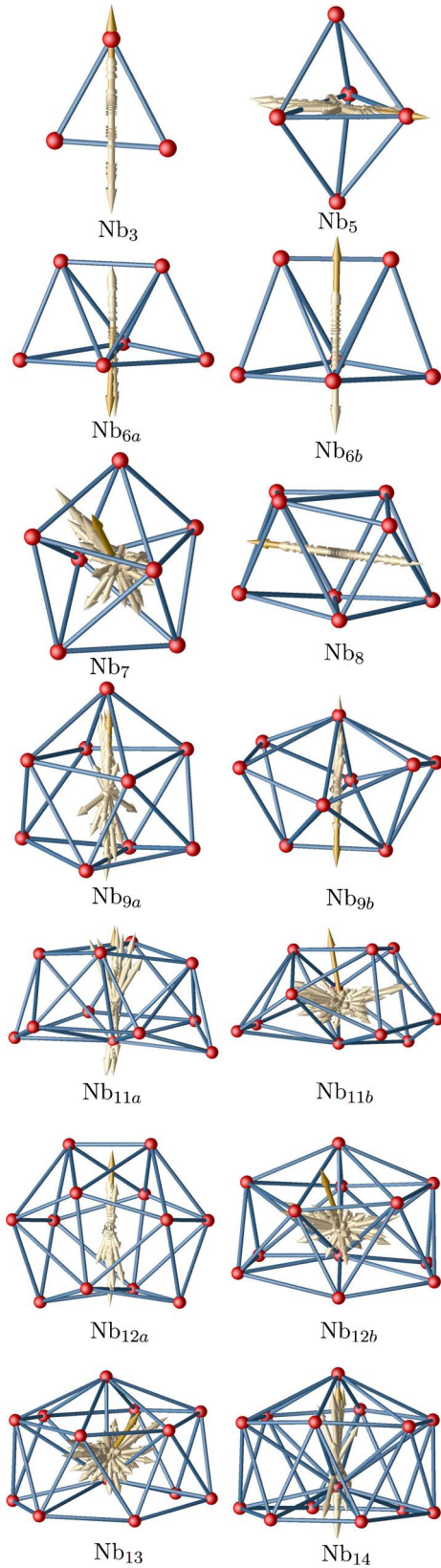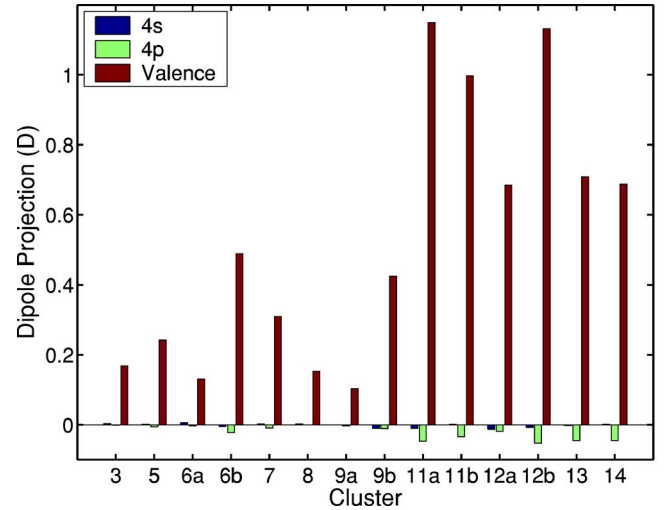
FIG. 8. (Color online) State decomposed dipole moment of the $4s$, $4p$, and valence states. The electric dipole moment is associated with the valence states, which are predominately of $4d$ character.

Because substantial cancellation occurs in the summation of the state decomposed moments, it is physically meaningful to separate the summation in (1) over states of atomic s, p, and d character

$$\boldsymbol{\mu} = \boldsymbol{\mu}_s^e + \boldsymbol{\mu}_p^e + \boldsymbol{\mu}_d^e. \tag{13}$$

(Remember $\boldsymbol{\mu}^{\text{ion}}=0$ has been imposed.) Figure 8 shows the projection of $\boldsymbol{\mu}_s^e$, $\boldsymbol{\mu}_p^e$, and $\boldsymbol{\mu}_d^e$ along the direction of the total dipole $\boldsymbol{\mu}$. For each cluster, these contributions are normalized to sum to μ. The predominant contribution to the electric dipole arises from the valence electrons, with some minor backward polarization from the semicore $4p$ states. This backward polarization is more predominate in clusters with a large moment (Nb_{11}-Nb_{14}); these clusters are also more asymmetric, which gives rise to more unusual chemical environments. Since the charge density of the $4s$ states is spherically symmetric around each ion, these states do not contribute to the electric dipole; that is, the center of "mass" of the $4s$ charge density coincides with the center of the nuclear charge.

For clusters with odd N, a spin moment results from the unpaired electron. All lowest energy, odd clusters studied have a spin moment of $1\mu_B$, in agreement with experiment[2] and previous calculations.[18] For these clusters, the analysis of the state decomposed electric moment can be carried further by separating the summation (1) over states of different spin

$$\boldsymbol{\mu} = \boldsymbol{\mu}_\uparrow^e + \boldsymbol{\mu}_\downarrow^e. \tag{14}$$

Figure 9 shows the projection of $\boldsymbol{\mu}_\uparrow^e$ and $\boldsymbol{\mu}_\downarrow^e$ along the direction of the total dipole for odd N clusters, again normalized to μ. A striking feature of the spin decomposition is that electric polarization of majority and minority spin states is often opposed. This is also seen in the spin density difference $\Delta\rho(\boldsymbol{r}) = \rho_\uparrow(\boldsymbol{r}) - \rho_\downarrow(\boldsymbol{r})$ shown in Fig. 11. Keeping electrons of opposite spin separate in real space maximizes the local spin

FIG. 7. (Color online) The state decomposed dipole moment. The tan vectors represent the dipole moment of each occupied electronic state. The total dipole moment is shown in gold. In general, the vector sum of these moments is nontrivial, but in some cases, a symmetry plane or axis is found.
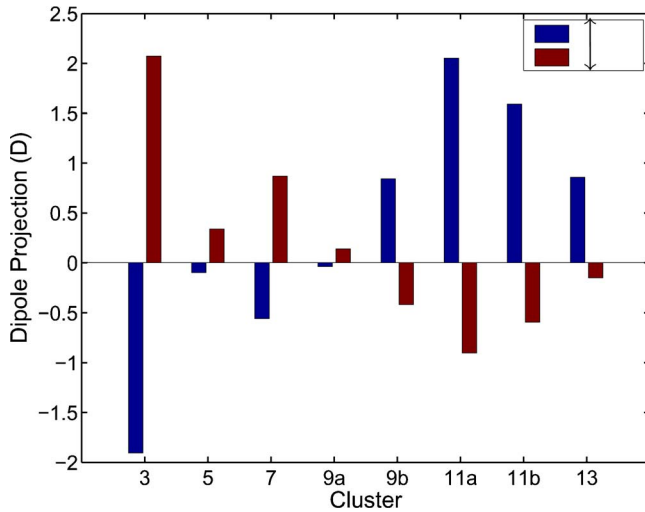
FIG. 9. (Color online) Spin decomposed electric dipole moment of the majority (↑) and minority (↓) spin. The separation of the spin density in real space, which causes the opposed electric moments, lowers the exchange energy of the cluster.

polarization and thus lowers the exchange energy of the cluster.

It is appealing to attribute the electric dipole of clusters with odd N to the unpaired electronic state. This is invalid, however, because it ignores the integrated nature of the dipole moment; all valence charge density (or states) must be included. To illustrate this, a cumulative sum $f(i)$ of the electric dipole over the valence states i

$$f(i) = f_0 + \hat{\boldsymbol{\mu}} \cdot \sum_{k\sigma}^{i} \boldsymbol{\mu}_{k\sigma}, \qquad (15)$$

is shown in Fig. 10 for Nb_{11a} and Nb_{12a}, where f_0 is the residual dipole of the $4s$ and $4p$ states. First, the effect of the unpaired electronic state [i.e., the last data point for Nb_{11a} in Fig. 10(a)] is no more significant than the highest energy, doubly degenerate state for Nb_{12}. Second, the cumulative sum fluctuates significantly, over 25 D in the case of Nb_{11a}. The energy range of the electronic states involved in this fluctuation is the occupied "bandwidth" of the Nb d states, which is approximately 4 eV for clusters of this size.

VI. SPIN DENSITY AND SPIN-ORBIT COUPLING

Recent Stern-Gerlach molecular beam experiments by Moro *et al.* have been interpreted in terms of a spin moment of odd N clusters that is uncoupled to the cluster (i.e., free to rotate) at low temperatures.[2] The coupling of the spin moment to the orientation of the cluster is mediated by the spin-orbit interaction; an uncoupled spin would imply that the magnetic anisotropy is much less than the rotational energy of the cluster ($\sim$1 meV) when formed at low temperatures.

A qualitative understanding of the coupling of the spin moment to the cluster can be obtained by looking at the spin density difference $\Delta\rho(\boldsymbol{r}) = \rho_\uparrow(\boldsymbol{r}) - \rho_\downarrow(\boldsymbol{r})$ shown in Fig. 11. For strong magnetocrystalline coupling, the spin would be ex-
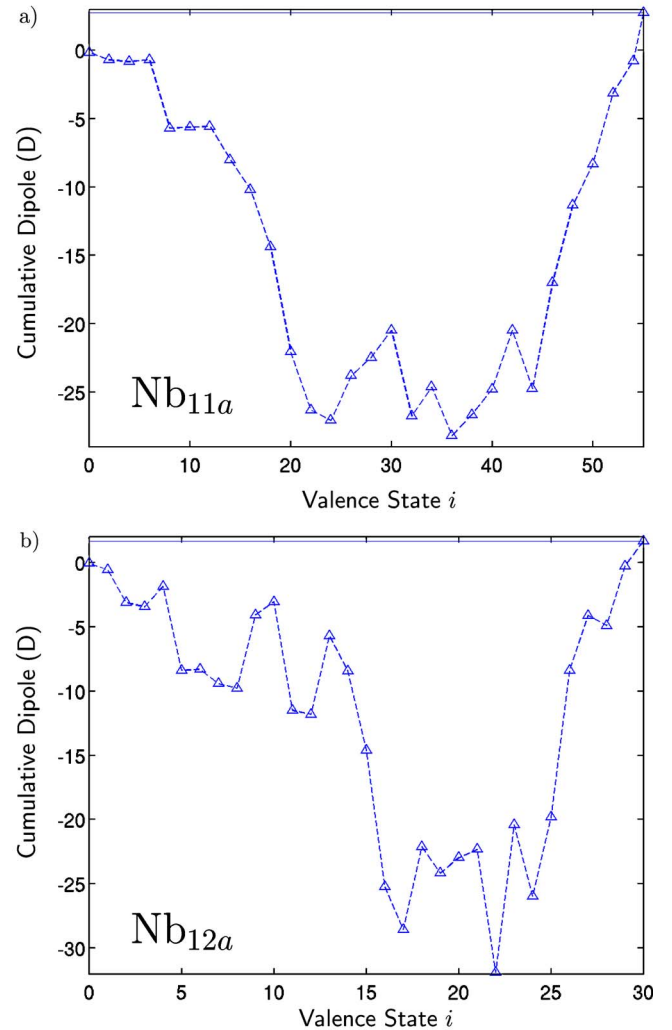

FIG. 10. (Color online) The cumulative dipole moment, including the charge density up to the ith valence state [Eq. (15)] for (a) Nb_{11a} and (b) Nb_{12a}.

pected to be localized to maximize the interaction with the orbital moment. Overall in Fig. 11, the spin moment is delocalized, being spread over several atoms in the cluster.

We have calculated the magnitude of the magnetic anisotropy in Nb_{11a} using the method described in Sec. II C. Several different quantization axes were investigated, including axes on a 5×5 uniform spherical grid, the principal axes of inertia, and the axis of the electric dipole moment. Using the spin moment aligned with the axis of the electric dipole as a reference, the difference in energy as the quantization axis of the spin moment was changed was found to be less than 0.25 meV. This is an order of magnitude less than the rotational kinetic energy $\frac{3}{2}k_B T$ at 20 K, which implies that the spin moment is uncoupled to the cluster and is free to interact with the applied magnetic field as is observed experimentally.[2]

VII. TEMPERATURE DEPENDENCE

Though the existence of the electric and spin moment in Nb clusters is well understood in terms of ground state, first-
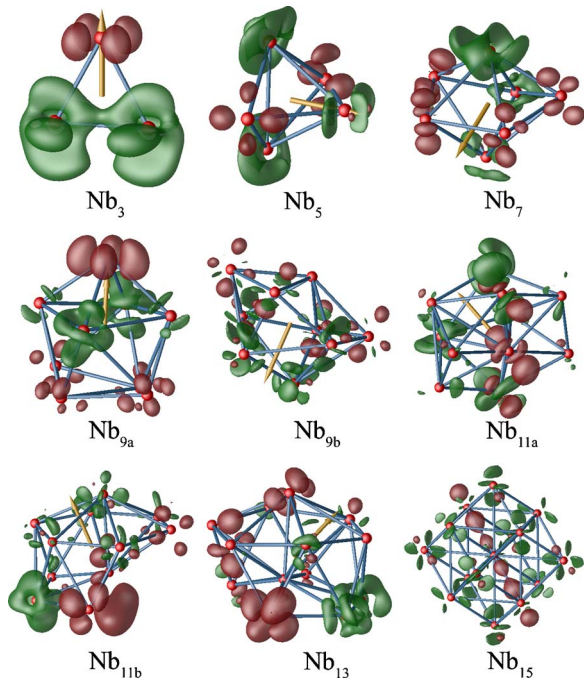
FIG. 11. (Color online) Spin density difference $\Delta\rho(\boldsymbol{r}) = \rho_{\uparrow}(\boldsymbol{r}) - \rho_{\downarrow}(\boldsymbol{r})$ for clusters with an odd number of electrons. Isosurfaces of spin up (down) character are shown in purple (green), and the gold vector represents the total dipole moment. Regions of primarily up or down character extend over several atoms in the cluster.

principles calculations, the temperature dependence of these moments is not. Section IV has established that the permanent electric dipole moment is related to asymmetry, and it is unlikely there is a structural transition (to higher symmetry) that occurs for *all* clusters at the same temperature, as needed to explain the experimental data.[1] Therefore, in this section, we focus on other possibilities.

The measurement of the electric dipole is based on the observation of the molecular beam deflection profiles after the clusters are passed through an inhomogeneous electric field. When the clusters are formed at high temperature (300 K), the profiles uniformly shift as the deflection field is turned on, due to the interaction of the induced moment and the inhomogeneous field.[1,36] At lower formation temperatures (20 K), however, the deflection profiles become asymmetric.[1]

Moro *et al.* have argued that the observed temperature dependence may be related to nascent superconductivity.[1,2] On the other hand, an excitation may occur as the temperature is raised that alters the electronic charge density enough to quench the electric dipole. For $N \approx 10$, an excitation energy of around 100 K is consistent with the experimental data.[1,2] In the following sections we investigate the effect of vibrational excitations on the electric dipole and the rotational dynamics of the cluster.

A. Vibrations

To quantify the influence of vibrations, we look at the vibrational spectra of Nb_{10} and Nb_{12b} clusters with a negli-
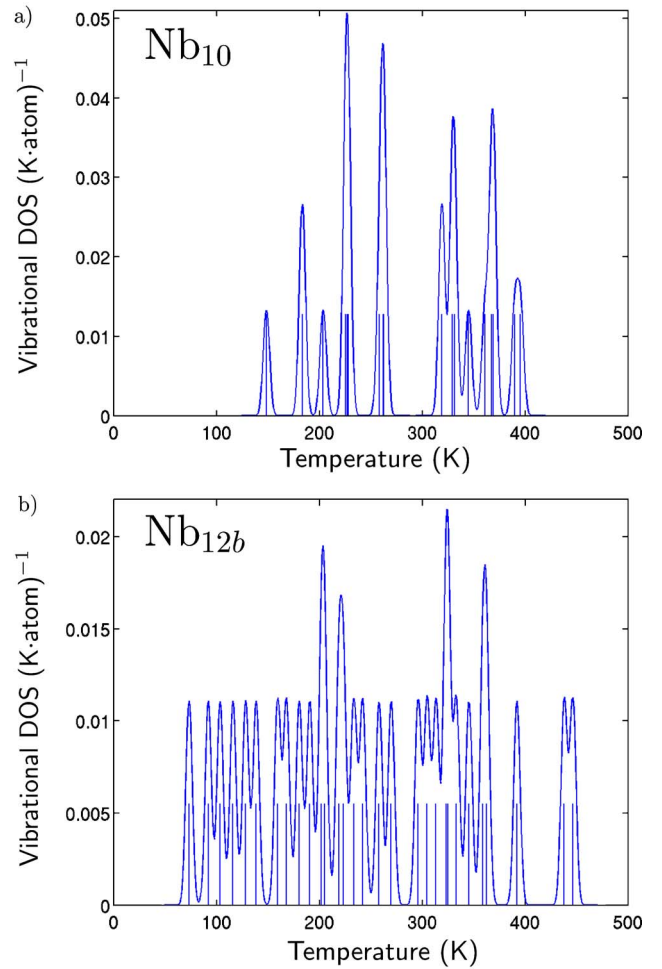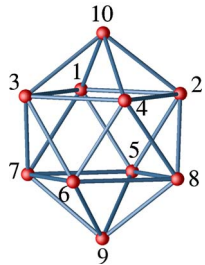

FIG. 12. (Color online) Vibrational density of states as a function of temperature for (a) Nb_{10} and (b) Nb_{12b}. The discrete spectrum (vertical lines) is broadened by a Gaussian with width 6 K (FWHM). For Nb_{12b}, although several vibrational excitations are possible near the experimentally observed critical temperature near 100 K (Ref. 1), the excitation of these states has little effect on the electric dipole.

gible and large (2.7 D) electric dipole, respectively. The vibrational density of states of these clusters as a function of temperature is shown in Fig. 12; for simplicity, the six zero energy modes which correspond to three independent translations and rotations are not shown.

The change in the electric dipole moment due to the atomic motion can be determined using the dynamical charge tensors $Z_{\alpha\beta}^n$ for each atom n. If the nth atom is displaced by $\boldsymbol{\tau}_n$, the change in the dipole moment is $\Delta\boldsymbol{\mu} = \Sigma_{n=1}^N \boldsymbol{Z}^n \boldsymbol{\tau}_n$.

Due to the low symmetry of the clusters, the tensors $\boldsymbol{Z}^n$ are not symmetric and can, therefore, not be decomposed into principal charges and directions. Physically, this implies that moving an atom in a direction $\boldsymbol{\tau}$ can result in a dipole moment oriented in a direction other than $\hat{\boldsymbol{\tau}}$. This can be characterized by the singular value decomposition $\boldsymbol{Z} = \boldsymbol{U}\boldsymbol{\Sigma}\boldsymbol{V}^{\dagger}$, in terms of the unitary matrices $\boldsymbol{U}$ and $\boldsymbol{V}$ and the real, diagonal matrix $\boldsymbol{\Sigma}$. This decomposition determines three orthogonal directions (the columns of $\boldsymbol{V}$) such that the change in the dipole moment (directions given by the col-

TABLE III. (Color online) Singular values $\sigma_1 \geqslant \sigma_2 \geqslant \sigma_3$ (e) of the dynamic charge tensor $\mathbf{Z}^n$ for the nth atom of Nb_{10}.

n	σ_1	σ_2	σ_3
1	0.20	0.07	0.01
2	0.20	0.07	0.01
3	0.20	0.07	0.01
4	0.20	0.07	0.01
5	0.19	0.07	0.01
6	0.19	0.07	0.01
7	0.19	0.07	0.01
8	0.19	0.07	0.01
9	0.25	0.25	0.10
10	0.25	0.25	0.10

TABLE IV. (Color online) Singular values $\sigma_1 \geqslant \sigma_2 \geqslant \sigma_3$ (e) of the dynamic charge tensor $\mathbf{Z}^n$ for the nth atom of Nb_{12b}.

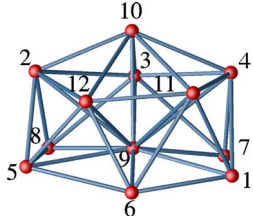| n	σ_1	σ_2	σ_3
1	0.30	0.19	0.08
2	0.50	0.22	0.10
3	0.70	0.23	0.03
4	0.32	0.20	0.12
5	0.33	0.24	0.10
6	0.74	0.15	0.03
7	0.47	0.25	0.14
8	0.39	0.28	0.05
9	0.92	0.35	0.01
10	0.38	0.15	0.04
11	0.32	0.19	0.04
12	0.36	0.17	0.05

umns of $\mathbf{U}$) is *maximized*. The magnitude of the dipole moment for a unit displacement is given by the singular values $\sigma_1 \geqslant \sigma_2 \geqslant \sigma_3 \geqslant 0.0$ of $\mathbf{Z}$, the diagonal elements of $\mathbf{\Sigma}$.

The singular values for Nb_{10} and Nb_{12b} are given in Tables III and IV. For Nb_{10}, the response of the two capping atoms ($n=9$ and 10) and the bases of the two square pyramids ($n=1-4$ and 5–8) react similarly to an applied electric field. The singular values are also smaller in comparison to Nb_{12b}, which is an indication that their vibrational contribution to the electric polarizability is small. Nb_{12b} has lower symmetry but contains a central, highly coordinated atom ($n=9$) with the largest singular value $\sigma_1 = 0.92e$. The electric dipole depends strongly on the movement of this atom because it is strongly bonded.

As the temperature is increased, vibrational modes can be excited, which will affect the cluster's electric dipole, and the dynamical charge tensors are able to quantify this change. For Nb_{12b}, six modes exist near the experimentally observed transition temperature ($\sim$100 K) with energies between 6 and 12 meV [see Fig. 12(b)]. However, the excitation of each of these modes results in only a minor change in the electric dipole of 0.1 D in magnitude and only a few degrees in direction. This is in agreement with previous frozen-phonon calculations.[9] Even when higher energy vibrational modes are considered, the change to the electric dipole remains small. This is because the ground state electronic density has "relaxed" to minimize the energy, and first order changes in the atomic positions are unable to significantly alter its distribution.

Additionally, molecular dynamics calculations have been performed at 100 K on Nb_{13}. The electric dipole moment was calculated at snapshots within the simulation. The ions were found to be displaced by 0.1–0.3 Å, with corresponding changes in bond lengths of less than 0.1 Å, and the electric dipole moment was found to change by only $\approx$0.01 D. This supports the conclusion that the change in the dipole moment due to vibrations at 100 K is small.

B. Rotations

The rotational dynamics of the cluster can potentially affect the experimental measurement of the electric dipole, and can be simulated using the methods of rigid body mechanics if the dipole is fixed to the cluster. Because distortions of the electronic density due to vibrations are small (see Sec. VII A), this is applicable for the electric dipole in Nb clusters.

An interesting analogy exists between the dynamics of an electric dipole fixed to a cluster and the dynamics of a "locked" magnetic dipole that occurs when the magnetoanisotropy energy is large. Indeed, the electric deflection profiles discussed below are qualitatively similar to the profiles seen in the magnetic deflection of Gd_N clusters,[37] which have a large magnetocrystalline anisotropy due to the significant spin-orbit interaction in rare earth elements and low site symmetry in clusters.

Classical simulations by Dugourd *et al.*,[38] using the thermal (Boltzmann) occupation of rotational states, were able to reproduce the molecular beam electric deflection of TiC_{60} clusters, but the temperature dependence was not studied. Such simulations are valid when the rotational energy spectrum is nearly continuous, that is, when $\langle I \rangle k_B T / \hbar^2 \gg 1$, where $\langle I \rangle$ is the average of the moments of inertia. For $N=12$ this
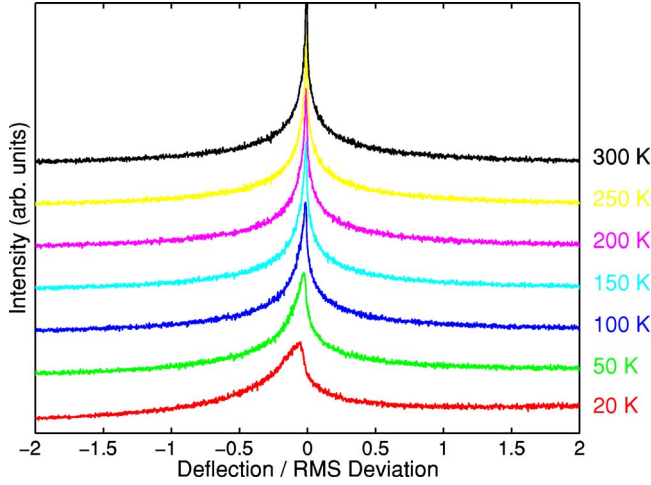
FIG. 13. (Color online) Simulations of the temperature dependence on the deflection of Nb_{12}, with a permanent electric dipole moment $\mu = 2\ D$, through an electric field $E = 80$ kV/cm and field gradient $E' = 170$ kV/cm^2. The asymmetry of the profile decreases as the temperature is raised.
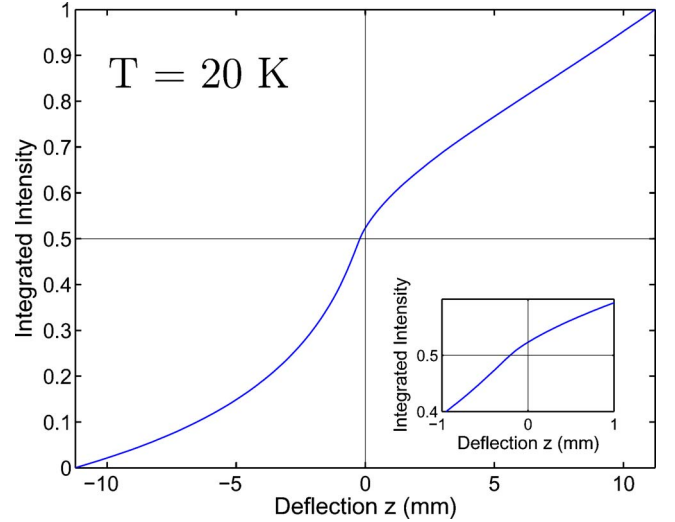

FIG. 14. (Color online) Integrated deflection profile for Nb_{12} at 20 K (the bottom profile of Fig. 13). The net displacement *against* the field may affect the measurement of the electric polarizability. Inset shows an enlargement of the curve near the origin. The width of the deflection (the scale of the z axis) is set by the geometric factor $K = 0.165$ m^2.

quantity is on the order of 10^3, so the discreteness of the energy level spectrum (spacing $\sim 10^{-5}$ eV) is negligible.

In general, the rigid body Hamiltonian can be written in terms of three Euler angles θ, ϕ, and ψ and three corresponding angular velocities $\dot{\theta}$, $\dot{\phi}$, and $\dot{\psi}$.[39] To obtain analytic solutions (to quadrature) two approximations are made. First, the cluster is modeled as a symmetric rigid body with inertial moments $I_1 = I_2 \neq I_3$. Within this approximation, the rigid body Hamiltonian depends on only four degrees of freedom: the angle θ, which designates the deviation of the electric dipole from a fixed axis z on the cluster (defined by the applied electric field), and three angular velocities $\dot{\theta}$, $\dot{\phi}$, and $\dot{\psi}$. Second, the adiabatic approximation is used such that $\langle \cos \theta \rangle$ is well defined. This is justified since the time spent interacting with the electric field, which is on the order of 1 ms, is much longer than the characteristic period of rotation, on the order of 10 ps.

With these approximations, it is possible to evaluate $\langle \cos \theta \rangle$ for a specific configuration of the cluster $k = \{\theta, \dot{\theta}, \dot{\phi}, \dot{\psi}\}$ using the method presented in Ref. 38. The intensity $I(z)$ for deflecting the cluster a distance z is then given by

$$I(z) = \frac{\sum_k \delta\left(z - \frac{K\mu E' \langle \cos \theta_k \rangle}{Mv^2}\right) \exp\left(-\frac{\mathcal{E}_k}{k_B T}\right)}{\sum_k \exp(-\mathcal{E}_k / k_B T)}, \quad (16)$$

where E' is the electric field gradient; M and v are the cluster's mass and velocity; $\mathcal{E}_k = \mathcal{E}_k(\theta, \dot{\theta}, \dot{\phi}, \dot{\psi})$ is the initial energy of the configuration (i.e., its kinetic energy); and K is a geometric factor that models the experimental apparatus. Equation (16) is a discrete approximation of Eq. (23) in Ref. 38.

Figure 13 shows the numerical evaluation of (16) for a dipole moment of $\mu = 2$ D at different temperatures T. For each profile, 10^7 configurations were sampled. Structural pa-

rameters $I_1 = I_2 = 45\ M_{Nb}\ Å^2$, $I_3 = 65\ M_{Nb}\ Å^2$, and $M = 12\ M_{Nb}$ were chosen to model Nb_{12}. Other parameters were chosen in accordance with experiment. The velocity v was adjusted linearly with temperature between $v = 300$ m/s ($T = 20$ K) and $v = 1100$ m/s ($T = 300$ K), and the magnitudes of the electric field E and field gradient E' were set to 80 kV/cm and 170 kV/cm^2, respectively.

Two points warrant further explanation. Because the velocity changes with temperature, the spread of the deflection profile also changes and is bounded by $|z| < K\mu E'/Mv^2$. In Fig. 13, the deflection profiles have been scaled by their RMS deviation to account for this broadening and to facilitate comparison between different temperatures. Also, in the evaluation of (16) the angular velocities $\{\dot{\theta}, \dot{\phi}, \dot{\psi}\}$ must be bounded. The average angular velocity determined by equipartition $\langle \omega \rangle = \sqrt{k_B T / \langle I \rangle}$ is used to restrict the magnitude of $\{\dot{\theta}, \dot{\phi}, \dot{\psi}\} \lesssim 5\langle \omega \rangle$.

There are two qualitative characteristics of the deflection profiles. First is the enhancement of asymmetry in the deflection profile at lower temperature. The asymmetry of the deflection profile is an experimental signature of a permanent electric dipole moment.[1] This is in contrast to the deflection of a cluster with no permanent moment, in which only a rigid shift (and no significant change in shape) of the deflection profile is caused by the induced electric moment. Further, the asymmetry of the profiles becomes less discernible as the temperature is increased, and is negligible in the profile at $T = 150$ K, above the experimentally observed transition.

In addition, there is a nonintuitive shift toward a lower field of the central peak at low temperature. This effect has also been observed in the deflection of TiC_{60} clusters with a permanent electric dipole moment.[38] The integration of the deflection profile at 20 K, shown in Fig. 14, shows that over half the intensity weight occurs on the left side of the profile.

In experiment, this shift is opposed by the induced dipole moment, which aligns with the field and would shift the deflection profiles to the right. The tendency of the permanent moment to shift the deflection profile to the left may explain the measurement of small and negative (for some cluster sizes) electric polarizabilities at low temperatures.[1]

However, not all of the features of the classical deflection agree with experiment. In particular, the overall width of the deflection profiles produced by these simulations is too large. This width is controlled by the geometric factor K, where $K \approx 0.3$ m^2 for the experimental apparatus of Ref. 1.[42] At 50 K, with a velocity of 385 m/s, this would produce a maximum width of over 1 cm. These large deflections would fall outside the range of the detector, however little loss in intensity is observed.[1]

In general, the asymmetry of the profile is determined by the ratio of electric and thermal energy $\mu E / k_B T$. An experimental test, in which the electric field E is varied, makes it possible to determine if the temperature dependence of the electric dipole is caused by a rigid body rotation. If the experimental transition temperature $T_c(N)$ is found to depend on the range of electric fields chosen in the experiment, then most likely the disappearance of the electric dipole is not an intrinsic effect, but instead caused by thermal averaging.

VIII. SUMMARY

First-principles electronic structure calculations have been used to explain many of the recent experimental observations on Nb$_N$. The calculated electric dipole moments are in good agreement with the experimental data. The strong correlation between structural asymmetry and the electric dipole moment, as quantified by the principal moments of inertia and charge deformation densities, supports the interpretation that the electric dipole has structural origin. Although the clusters are homonuclear and directional bonding between Nb d electrons is largely covalent, some polar character—and hence charge transfer—does occur because of the presence of inequivalent sites and contributes to the development of an electric dipole. Furthermore, these calculations find that clusters with an odd number of electrons have a spin moment of $1\mu_B$ that is uncoupled to the cluster because magnetocrystalline anisotropy is an order of magnitude smaller than the rotational energy of the cluster.

The positive surface energy leads to the expectation that clusters will become more symmetric as N increases. It is an open question whether the asymmetry is able to explain the electric dipole moment observed in clusters containing hundreds of atoms. However, even at these "large" sizes almost all the atoms are on the surface which may lead to symmetry lowering reconstructions.

Beyond the origin of the electric dipole is its observed temperature dependence. Analysis of the linear response of the electronic charge density with respect to atomic displacements and homogeneous electric fields rule out the excitation of vibrational modes as a cause of this disappearance. A lingering possibility is that clusters formed at low temperature, with less energy available to anneal, may contain different isomers than those formed at higher temperatures. This question can be addressed experimentally by selecting equal velocity clusters with identical N, formed at different temperatures, and comparing their deflection profiles.

The correlated temperature dependence of the electronic and spin moment points to a common origin. However, since spin-orbit coupling is small, these degrees of freedom should be independent. One explanation for their common behavior is the effect of thermal averaging caused by the rotational dynamics in the molecular beam. Although unable to explain the width of the deflection profiles, the asymmetry in the profiles is increased at lower temperatures as observed. The proposed experiment, in which the magnitude of the applied homogenous electric field is changed, should be able to determine if rotational dynamics is important in the interpretation of the experimental data. If so, then one would expect that low temperature molecular beam experiments may reveal additional phenomena in a large number of other nanosystems that before were masked by thermal averaging. However, the simultaneous presence of isomers and their relative abundances would need to be considered to fully understand the deflection profiles.

*Electronic address: pickett@physics.ucdavis.edu

[1] R. Moro, X. Xu, S. Yin, and W. A. de Heer, Science **300**, 1265 (2003).

[2] R. Moro, S. Yin, X. Xu, and W. A. de Heer, Phys. Rev. Lett. **93**, 086803 (2004).

[3] A. F. Andreev, J. Supercond. **12**, 197 (1999).

[4] D. C. Ralph, C. T. Black, and M. Tinkham, Phys. Rev. Lett. **74**, 3241 (1995).

[5] W. P. Halperin, Rev. Mod. Phys. **58**, 533 (1986).

[6] C. D. Batista, J. E. Gubernatis, J. Bonča, and H. Q. Lin, Phys. Rev. Lett. **92**, 187601 (2004).

[7] P. B. Allen, J. Chem. Phys. **120**, 2951 (2004).

[8] P. B. Allen, A. G. Abanov, and R. Requist, Phys. Rev. A **71**, 043203 (2005).

[9] K. E. Andersen, V. Kumar, Y. Kawazoe, and W. E. Pickett, Phys. Rev. Lett. **93**, 246105 (2004); **95**, 089901 (2005).

[10] W. Fa, C. Luo, and J. Dong, Phys. Rev. B **71**, 245415 (2005).

[11] X. Gonze, J.-M. Beuken, R. Caracas, F. Detraux, M. Fuchs, G.-M. Rignanese, L. Sindic, M. Verstraete, G. Zerah, and F. Jollet, Comput. Mater. Sci. **25**, 478 (2002), URL http://www.abinit.org.

[12] S. Goedecker, SIAM J. Sci. Comput. (USA) **18**, 1605 (1997).

[13] M. C. Payne, M. P. Teter, D. C. Allan, T. A. Arias, and J. D. Joannopoulos, Rev. Mod. Phys. **64**, 1045 (1992).

[14] X. Gonze, Phys. Rev. B **54**, 4383 (1996).

[15] J. P. Perdew, K. Burke, and M. Ernzerhof, Phys. Rev. Lett. **77**, 3865 (1996).

[16] M. Fuchs and M. Scheffler, Comput. Phys. Commun. **119**, 67 (1999), URL http://www.fhi-berlin.mpg.de/th/fhi98md/fhi98PP/.

[17] N. Troullier and J. L. Martins, Phys. Rev. B **43**, 1993 (1991).

[18] V. Kumar and Y. Kawazoe, Phys. Rev. B **65**, 125403 (2002).

[19] M. R. Zakin, R. O. Brickman, D. M. Cox, and A. Kaldor, J. Chem. Phys. **88**, 3555 (1988).

[20] Y. Hamrick, S. Taylor, G. W. Lemire, Z.-W. Fu, J.-C. Shui, and M. D. Morse, J. Chem. Phys. **88**, 4095 (1988).

[21] Y. M. Hamrick and M. D. Morse, J. Phys. Chem. **93**, 6494 (1989).

[22] M. B. Knickelbein and S. Yang, J. Chem. Phys. **93**, 1476 (1990).

[23] M. B. Knickelbein and S. Yang, J. Chem. Phys. **93**, 5760 (1990).

[24] M. R. Zakin, D. M. Cox, and A. Kaldor, J. Phys. Chem. **91**, 5224 (1987).

[25] J. L. Elkind, F. D. Weiss, J. M. Alford, R. T. Laaksonen, and R. E. Smalley, J. Chem. Phys. **88**, 5215 (1988).

[26] H. Grönbeck and A. Rosén, Phys. Rev. B **54**, 1549 (1996).

[27] H. Grönbeck, A. Rosén, and W. Andreoni, Phys. Rev. A **58**, 4630 (1998).

[28] V. Kumar Comput. Mater. Sci. **35**, 375 (2006).

[29] X. Gonze, Phys. Rev. B **55**, 10337 (1997).

[30] X. Gonze and C. Lee, Phys. Rev. B **55**, 10355 (1997).

[31] P. E. Blöchl, Phys. Rev. B **50**, 17953 (1994).

[32] G. Kresse and D. Joubert, Phys. Rev. B **59**, 1758 (1999).

[33] G. Kresse and J. Furthmüller, Comput. Mater. Sci. **6**, 15 (1996).

[34] G. Kresse and J. Furthmüller, Phys. Rev. B **54**, 11169 (1996).

[35] L. Goodwin and D. R. Salahub, Phys. Rev. A **47**, R774 (1993).

[36] M. B. Knickelbein, J. Chem. Phys. **118**, 6230 (2003).

[37] D. C. Douglass, J. P. Bucher, and L. A. Bloomfield, Phys. Rev. Lett. **68**, 1774 (1992).

[38] P. Dugourd, I. Compagnon, F. Lepine, R. Antoine, D. Rayane, and M. Broyer, Chem. Phys. Lett. **336**, 511 (2001).

[39] H. Goldstein, C. P. Poole, and J. L. Safko, *Classical Mechanics*, 3rd ed. (Addison Wesley, Reading, MA, 2002).

[40] Convergence of the self-consistent iteration was improved using the preconditioning parameters ediemac=3.0 and emix=0.5.

[41] The higher energy $N=13$ structure is not discussed further, since its binding energy is over 30 meV/atom lower than the structure used in this work.

[42] W. A. de Heer (private communication).